Earth, Planets and Space

FULL PAPER Open Access

Investigations of the degree of asymmetry across the dayside magnetopause under southward interplanetary magnetic field using GEOTAIL observations

Koji Kondoh[1*] and Shin-ya Nitta[2,3,4]

Abstract

The magnetic reconnection environment around the dayside geomagnetopause under long-lasting southward interplanetary magnetic field (IMF) conditions is investigated using the in-situ observation by GEOTAIL satellite from 1994 to 2019. We focus on the degrees of asymmetry in the plasma density, ion temperature and the magnetic field strength between both sides of the magnetopause, that is, the ratio of the value in the magnetosphere to that in the magnetosheath in order to compute the much more realistic current sheet systems in numerical simulations. To exclude all of the interplanetary disturbance events such as Corotating Interaction Regions (CIRs) and Coronal Mass Ejections (CMEs), we investigate magnetopause crossings under long-lasting southward IMF conditions. GEOTAIL satellite sometimes repeatedly across the magnetopause during each pass due to the oscillating of the magnetopause. The degrees of asymmetry vary even during a single pass. This variation depends on the locus of the observation point, particularly the GSM Y-position, not on the time. The degrees of asymmetry in the plasma density, ion temperature and the magnetic field strength have significant variation in the data. The data points of the degree of asymmetry in the plasma density significantly spread in the duskside, while that in the magnetic field strength further widely spread in the dawnside. The degree of asymmetry in the plasma density and that in the magnetic field strength have fixed negative correlation on a log–log scale.

Keywords GEOTAIL satellite, Asymmetric magnetic reconnection, Magnetohydrodynamics (MHD) simulation, Magnetopause, In-situ observation

*Correspondence:
Koji Kondoh
kondo@cosmos.ehime-u.ac.jp
Full list of author information is available at the end of the article

Graphical Abstract

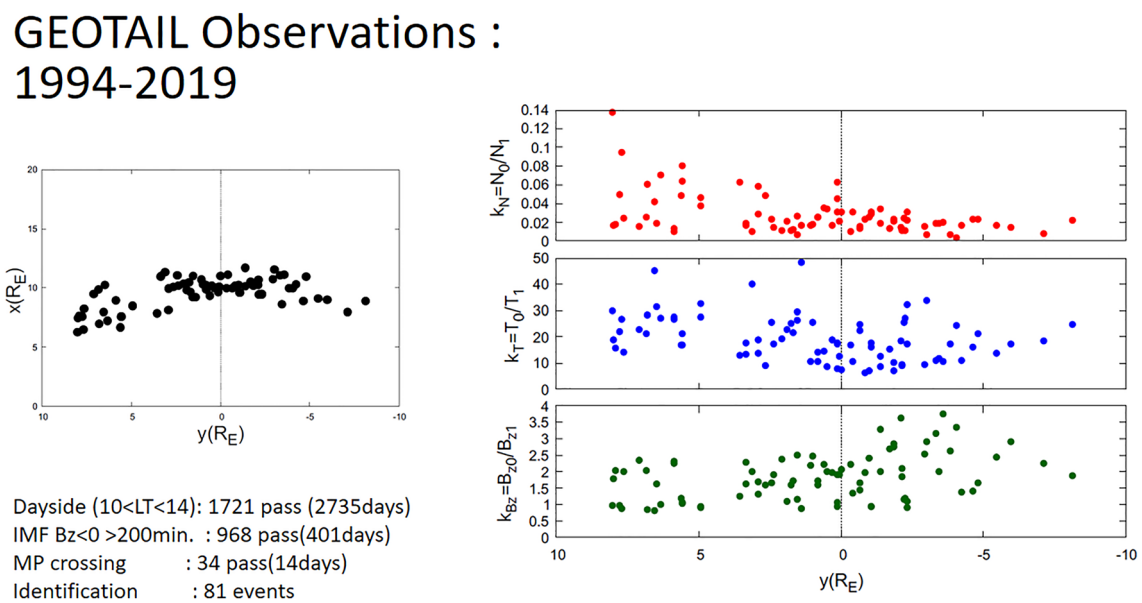

Introduction

There is compelling observational evidence that magnetic reconnection plays a major role in the dynamics of the solar corona and the planetary magnetosphere (Parker 1963; Tsuneta 1996; Paschmann et al. 1979; Gosling et al. 1986). Large explosion events such as coronal mass ejection and magnetic reconnection in the magnetotail seem to be associated with symmetric reconnection (Tsuneta 1996; Gosling et al. 1986). On the other hand, small solar flares and flux transfer events in the dayside magnetopause are associated with asymmetric reconnection (Chen et al. 2014; Paschmann et al. 1979).

Asymmetric reconnection has been studied by a lot of researchers (Petschek and Throne 1967; Hoshino and Nishida 1983; Lin and Lee 1993; Kondoh et al. 2004; Cassak and Shay 2007). However, these studies focused on the jet region or the region around the X-point. To understand the spontaneous reconnection system, we must consider the entire reconnection system. Then, we have shown that the entire structure of the asymmetric reconnection is drastically different from the symmetric case even for slight magnetic asymmetry (Nitta et al. 2016; Nitta and Kondoh 2019, 2021, 2022). However, our previous studies have been done on the assumption of the initial isothermal condition for simplicity.

We need to set up much realistic initial conditions to verify our model. Geo-magnetopause is presently the most accessible natural plasma environment where magnetic reconnections and the consequential phenomena can be measured in situ (Archer et al. 2019; Ivchenko et al. 2000; Hasegawa et al. 2003; Phan et al. 2001; Teh and Hau 2004). Then, it is suitable that we apply our model to the asymmetric reconnection in the dayside geo-magnetopause. Phan et al. (2013) showed using THEMIS observations that the majority of reconnection events occurred for the small difference of plasma β on both sides of the current sheet, and the majority of reconnection events occurred over a large range of the degree of magnetic shears. Walsh et al. (2012) investigated a dawn–dusk asymmetry in plasma parameters within the geo-magnetosheath using statistical observations by the THEMIS spacecrafts. They showed the ion density and temperature are greater on the dawnside while the magnetic field strength and bulk flow speed are greater on the duskside.

The main purpose of this paper is to investigate the asymmetric reconnection environment near the ecliptic plane in the dayside magnetopause and evaluate the validation of the initial conditions in the numerical simulations. For these purposes, we identify the

magnetopause crossing events by GEOTAIL satellite in the long-lasting southward IMF condition to exclude disturbed events. Then, we investigate the temporal and spatial variation of the ratio of the magnetic strength, the plasma density and the ion temperature between both sides of the magnetopause.

Dataset

We used data obtained by the low-energy particle experiment (LEP) (Mukai et al. 1994) and the magnetic field experiment (MGF) (Kokubun et al. 1994) on board GEOTAIL spacecraft from 1994 to 2019. Plasma moments such as the number density, the ion temperature, and the plasma velocity are calculated under the assumption that all ions are protons. We used 12 s (four-spin) averaged data for magnetic field vectors. In this study, GEOTAIL data were used when the spacecraft was located in the region within $10 < \mathrm{MLT} < 14$ and when the southward interplanetary magnetic field (IMF) data from OMNI base (https://spdf.gsfc.nasa.gov/pub/data/omni/high_res_omni) continued for at least 200 min. These OMNI data have been shifted from spacecraft positions of observation to the bow shock nose. We identified 81 complete magnetopause crossing events. Partial magnetopause crossing in which the spacecraft did not fully traverse the magnetopause is not included.

Results and discussion

Typical high magnetic asymmetry condition

We investigate a case study of a typical dayside magnetopause environment observed on 26 April 2009. Temporal variations in the IMF B_z from OMNI database and in the number density N (second panel), the ion temperature T (third panel) and the z-component of the magnetic field B_z (bottom panel) from GEOTAIL satellite between 20:30 and 23:45 UT are plotted in Fig. 1. The seven periods shown by the vertical yellow (magnetosheath side) and light blue (magnetosphere side) solid lines are identified as the magnetopause crossings by GEOTAIL satellite. The magnetopause crossings are repeatedly observed by GEOTAIL satellite in this single pass, such events are hereafter referred to as "series event" in this paper. We limit the analysis period when the southward IMF B_z at the bow shock nose continues over 200 min; therefore, the IMF B_z shown in the top panel is negative all the time in this figure. Temporal variation of the degree of asymmetry in the number density $k_N = N_0/N_1$ (top panel), the temperature $k_T = T_0/T_1$ (middle panel) and the z-component of the magnetic field $k_{B_z} = B_{z0}/B_{z1}$ (bottom panel) between 20:30 and 23:45 UT from GEOTAIL satellite are plotted in Fig. 2. We averaged 5 points (1 min.) data at each line in the previous figure and the subscript 0 and 1 indicates that the value was observed in the magnetosphere and the magnetosheath, respectively. The time indicated in this figure is the observation time of the five points used for the average of the value in the magnetosheath as indicated by the yellow vertical line in Fig. 1. In this series event, $k_N \lesssim 0.02$, $k_T \sim 10$, and $\mathrm{k_{B_z}} \gtrsim 2.0$ all the time. This cold dense plasma condition in the magnetosheath in contrast with that in the magnetosphere is typical. It is also found that k_{B_z} gradually decreases until 22:00 and then keeps about 2.5. From only this figure, it is

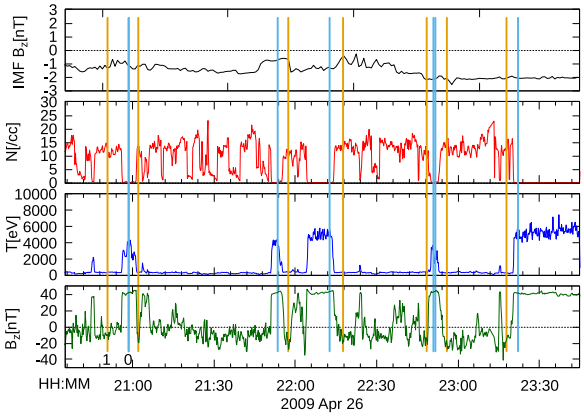

Fig. 1 Temporal variation in the IMF B_z (top panel) from OMNI database and in the number density N (second panel), the ion temperature T (third panel) and the z-component of the magnetic field B_z (bottom panel) observed by GEOTAIL satellite on 26 April 2009. The vertical solid lines show the time when we averaged 5-point (1 min.) values in the magnetosphere (orange lines) and the magnetosheath (light blue lines), respectively

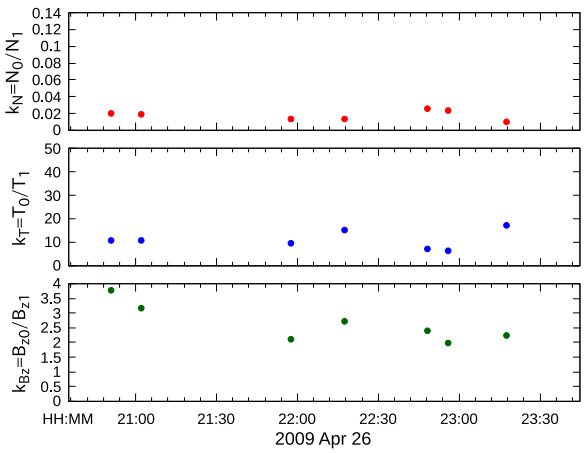

Fig. 2 Temporal variation in the degrees of asymmetry in the number density $k_N = N_0/N_1$ (top panel), the ion temperature $k_T = T_0/T_1$ (middle panel) and the z-component of the magnetic field $k_{B_z} = B_{z0}/B_{z1}$ (bottom panel) observed by GEOTAIL satellite on 26 April 2009. The subscript 0 and 1 show the value observed in the magnetosphere and the magnetosheath, respectively

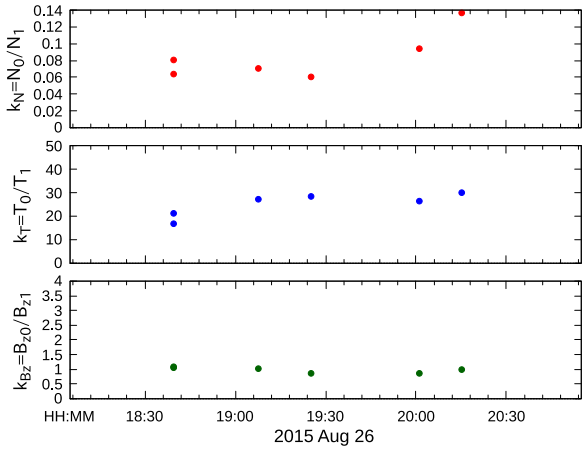

Fig. 3 Temporal variation in the degrees of asymmetry observed by GEOTAIL satellite on 26 August 2015. The format is the same as in Fig. 2

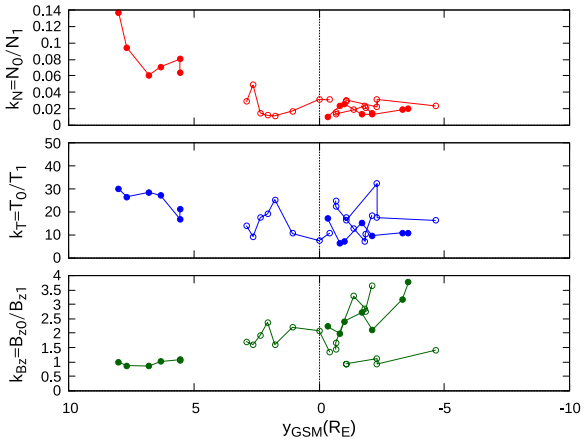

Fig. 4 Plot of the degree of asymmetry k_N, k_T and k_{B_z} as a function of y_{GSM} in five series events. The magnetopause crossings were repeatedly observed in a single pass. Such events are referred to as "series events" in this paper. The k_N is large on the dusk side, whereas the k_{B_z} on the dawn side

not impossible to determine whether this is temporal or spatial variation.

Weak magnetic asymmetry condition

Next, we show another case study of the almost magnetically symmetric dayside magnetopause environment observed on 26 August 2015. The same parameters as in Fig. 2 between 18:00 and 21:00 UT from GEOTAIL satellite are plotted in Fig. 3. In this series event, six magnetopause crossings by GEOTAIL satellite are identified, and all of k_{B_z} in these crossings are almost 1.0. That is, the dayside magnetopause in this period was magnetically symmetric. The number density and ion temperature remain to be weakly asymmetric. k_N gradually increases after the magnetopause crossing at 19:30. From only this figure, it is also not impossible to determine whether this is a temporal or spatial variation.

Series events

For further investigation of the temporal and spatial variation of the series events, we plot k_N, k_T, and k_{B_z} in the five series events, which are identified over five magnetopause crossings, including the above two events (plotted with filled circles) with respect to the GSM Y-position in Fig. 4. One single series event is shown by a plot set connected with solid lines. Note that GEOTAIL satellite moves toward positive y-direction. These five series events show spatial dependence, rather than temporal one. The asymmetry parameters k_N and k_T enhance in the positive y-position, while k_{B_z} in the negative y-position. The little temporal dependence in the asymmetry parameters means that the motions of the magnetopause, which allows us to observe the multiple magnetopause crossings, have little impact on the magnetopause condition.

All events

To confirm the above dependence, we plot the asymmetry parameters of all 81 events with respect to the y-position in Fig. 5. Every parameter does not necessarily depend on the y-position; however, the spread in the data of these parameters depends on it. Particularly, k_N significantly spread in the positive y-position, while k_{B_z} spread in the negative y-position.

Next, we check the range of these degrees of asymmetry. The degrees of asymmetry in the number density shown in the top panel distribute $0.01 \leq k_N \leq 0.14$ on the dusk side, while $k_N \sim 0.01$ on the dawn side. The degrees of asymmetry in ion temperature shown in the middle panel distribute $k_T \sim 20$ in all y-position. The degrees of asymmetry in the z-component of the magnetic field shown in the bottom panel distribute $0.5 < k_{B_z} < 2.5$ on the dusk side, while wide $1.0 \leq k_{B_z} < 4$ on the dawn side.

Relationship between asymmetry parameters

To investigate the above opposite dependency on the y-position and the relationship between k_N and k_{B_z}, we show scatterplot of k_N versus k_{B_z} in Fig. 6. This scatterplot has a fixed negative correlation on a log–log scale. In the iso-thermal equilibrium condition used in our previous studies, the degree of asymmetry in the plasma density satisfies

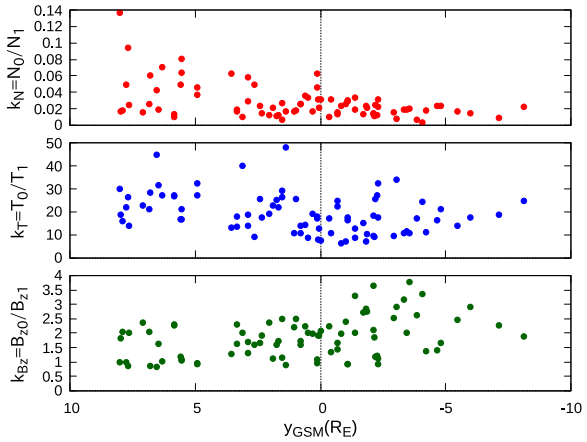

Fig. 5 Plot of the degree of asymmetry k_N, k_T and k_{B_z} as a function of y_{GSM} in all 81 crossings. The spread in the data of the k_N is large on the dusk side, whereas that of the k_{B_z} on the dawn side

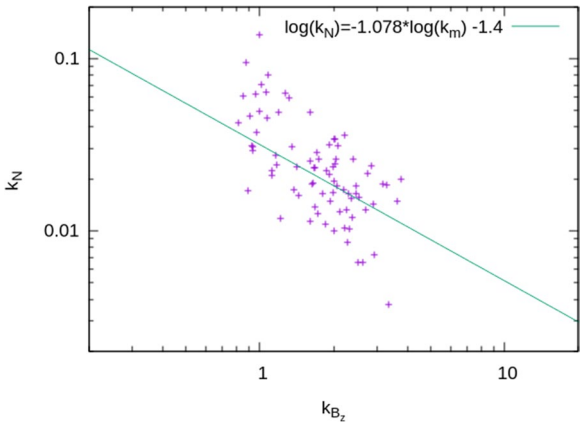

Fig. 6 Scatterplot of k_N versus k_{B_z} in the all crossings on a log–log scale

$$k_N = \frac{\beta_0}{k_{B_z}^2(1+\beta_0)-1}k_{B_z}^2,$$

where β_0 is the plasma beta value on the low beta side. This scatter plot does not satisfy this relationship.

As mentioned in the introduction, Walsh et al. (2012) investigated a y-position dependency in the dayside magnetosheath and showed the ion density and temperature are greater on the dawnside while the magnetic field strength is greater on the dusk side in the magnetosheath. Then, they concluded that their results were consistent with the expected dependencies that would result from the interactions of the Parker spiral interplanetary magnetic field with the Earth's bow shock.

Conclusions

We investigated the magnetopause environment near the ecliptic plane using the observational data from GEOTAIL satellite during the long-lasting negative IMF B_z component near the bow shock-nose. We focused on the degree of asymmetry on both sides of the current sheet in the dayside magnetopause near the sub-solar point. Our previous studies using numerical simulations showed that these asymmetries cause asymmetric magnetic reconnection and affect the global reconnection structure (Nitta et al. 2016; Nitta and Kondoh 2019, 2021, 2022). The repeated crossings of the magnetopause by GEOTAIL satellite during a single pass, which we call as "series event", due to the oscillating motion of the magnetopause allowed us to continuously investigate these environments.

In these series events, we found a magnetically symmetric environment with ($k_{B_z} \sim 1$) relative to the magnetopause layer (current sheet), not only the typical cold dense plasma environment in the magnetosheath compared with that in the magnetosphere ($k_{B_z} > 1$). Even in a single series event, the degree of asymmetry varies. This is the spatial variation, not the temporal one. This variation depends on the GSM-Y position. Every degree of asymmetry k has the spread in the data, and the spread depends on the GSM Y-position. The degree of asymmetry in the plasma density k_N has a fixed negative correlation with that in the magnetic field strength k_{B_z} on a log–log scale. In future work, we will investigate the asymmetric reconnection evolutions in these realistic degrees of asymmetry conditions.

Appendix: Information of All 81 magnetopause crossings

Information of the all events.

See Table 1

Table 1 The observation time, ion number density, B_z component and the satellite GSM position on both sides of the magnetopause

Time1	*N*1	*T*1	Bz1	*x*	*y*	*z*	Time0	*N*0	*T*0	Bz0	*x*	*y*	*z*
1995-10-25-6-11-57.000000	28.285	132.6	−20.582	11.324	3.098	0.026	1995-10-25-6-36-52.500000	0.2826	5295.3	41.296	10.984	3.598	−0.262
1995-10-25-8-41-18.500000	42.1466	151.5	−18.568	8.936	5.844	−1.776	1995-10-25-8-33-49.750000	0.559	4043.9	42.118	9.078	5.72	−1.686
1995-10-25-8-41-18.500000	42.1466	151.5	−18.568	8.936	5.844	−1.776	1995-10-25-8-49-37.250000	0.4338	4148.5	43.024	8.778	5.984	−1.876
1996-1-3-1-43-46.718750	25.938	258.1	−35.862	9.634	1.68	1.57	1996-1-3-2-17-2.625000	0.3262	5639.7	61.618	9.484	2.644	1.71
1996-3-7-6-37-15.000000	20.0446	145.1	−31.89	10.308	−4.218	−0.572	1996-3-7-6-21-44.375000	0.3472	1629.6	43.814	10.066	−4.536	−0.704
1996-11-28-10-30-40.750000	12.1946	229.8	−32.502	11.118	−0.422	1.554	1996-11-28-10-35-59.000000	0.3758	2471.9	43.86	11.09	−0.298	1.506
1996-11-28-10-47-49.250000	8.6912	312.5	−20.376	11.022	−0.002	1.4	1996-11-28-10-43-32.250000	0.2724	2358.4	42.456	11.05	−0.112	1.438
1996-11-28-11-32-5.500000	9.6992	366.8	−23.402	10.702	1.062	0.988	1996-11-28-11-45-58.250000	0.167	3893.9	51.534	10.592	1.392	0.862
1996-11-28-12-1-16.250000	14.429	218	−30.916	10.448	1.762	0.728	1996-11-28-11-54-44.500000	0.1648	5523.8	49.6	10.512	1.602	0.788
1996-11-28-12-13-30.500000	14.985	334.9	−20.794	10.334	2.052	0.622	1996-11-28-12-17-47.500000	0.1784	6411.8	49.462	10.292	2.158	0.588
1996-11-28-12-25-32.750000	16.571	256.7	−27.4	10.208	2.342	0.526	1996-11-28-12-20-39.250000	0.2454	4508.8	52.992	10.264	2.228	0.564
1996-11-28-12-37-35.500000	19.0832	284.8	−33.796	10.076	2.632	0.43	1996-11-28-12-34-43.750000	0.9334	2659	54.164	10.108	2.562	0.452
1996-11-28-12-48-48.500000	14.9818	305.4	−32.554	9.944	2.892	0.34	1996-11-28-12-46-33.750000	0.4296	4252.8	55.494	9.972	2.842	0.358
1997-1-15-8-46-57.875000	22.566	130.5	−24.218	7.942	−7.102	0.99	1997-1-15-8-54-50.250000	0.194	2430.1	55.176	8.038	−6.908	1.014
1997-1-20-19-45-38.000000	32.1316	260.7	−37.664	9.45	−2.138	0.31	1997-1-20-19-42-48.625000	0.3522	2369.9	69.778	9.434	−2.214	0.29
1997-12-11-7-21-48.625000	14.5602	98.7	−29.64	10.96	−4.792	2.31	1997-12-11-7-24-51.375000	0.3396	2110.3	49.598	10.964	−4.712	2.3
1997-12-11-11-40-24.625000	13.8648	177.7	−41.43	9.806	1.882	0.698	1997-12-11-11-42-38.625000	0.2916	4065.7	46.404	9.782	1.938	0.68
1998-3-15-0-14-30.500000	26.9558	277.5	−36.748	8.596	−3.438	−1.742	1998-3-15-0-9-38.250000	0.5246	3266.4	73.622	8.524	−3.548	−1.804
1998-5-26-17-26-43.250000	9.0814	103	−18.822	8.864	−8.108	−2.64	1998-5-26-16-55-38.750000	0.2028	2538.5	35.312	8.15	−8.492	−2.366
1999-1-4-6-29-32.031250	14.1462	174.4	−25.936	9.342	0.596	1.12	1999-1-4-6-44-34.125000	0.5088	2539.2	57.672	9.224	1.042	1.06
1999-4-8-6-17-2.062500	30.9566	167	−20.53	10.98	1.528	−0.74	1999-4-8-6-13-22.625000	0.2024	4425.2	51.466	10.96	1.432	−0.758
2000-5-18-5-52-8.875000	7.7418	538.8	−25.616	11.688	−1.378	−2.388	2000-5-18-5-39-21.250000	0.2624	4631	51.548	11.522	−1.632	−2.41
2000-5-28-15-34-40.250000	17.1674	164.3	−14.996	11.564	−3.018	−2.482	2000-5-28-15-22-16.750000	0.1244	5567.1	43.838	11.374	−3.282	−2.44
2001-2-2-2-43-20.906250	18.732	276.4	−13.354	9.98	−4.052	−0.54	2001-2-2-2-47-0.250000	0.0698	6727.8	44.854	9.99	−3.958	−0.508
2001-2-2-2-51-40.500000	15.0196	312.2	−18.16	9.99	−3.834	−0.466	2001-2-2-2-48-49.890625	0.0984	5418.8	47.664	9.99	−3.912	−0.49
2001-5-7-8-27-50.375000	14.0726	189.4	−51.692	9.44	−2.262	−2.062	2001-5-7-8-21-56.187500	0.1654	5159.1	62.616	9.356	−2.412	−2.08
2001-5-7-8-30-16.562500	12.6556	157	−46.864	9.474	−2.202	−2.06	2001-5-7-8-33-55.875000	0.3046	4021.1	54.774	9.516	−2.112	−2.05
2002-2-2-3-34-7.437500	13.1922	268.2	−55.1	6.678	5.584	0.95	2002-2-2-3-29-27.265625	0.6438	4548.8	65.67	6.782	5.478	0.95
2002-2-22-16-24-15.625000	15.1396	212	−17.128	9.016	−5.97	−1.81	2002-2-22-16-19-59.750000	0.2152	3688.8	49.966	8.99	−6.09	−1.81
2002-2-22-16-42-56.375000	12.882	194.9	−20.126	9.114	−5.458	−1.81	2002-2-22-16-50-14.750000	0.213	2696	49.576	9.15	−5.252	−1.8
2002-12-21-22-54-29.250000	11.087	280.5	−21.476	8.242	7.624	0.52	2002-12-21-23-6-15.625000	0.2724	3967.8	43.38	7.958	7.758	0.51
2002-12-21-23-19-14.750000	17.5602	200.7	−21.388	7.638	7.902	0.5	2002-12-21-23-14-47.000000	0.3208	3205.1	44.064	7.752	7.852	0.508
2002-12-21-23-26-33.375000	17.9874	179.3	−26.408	7.458	7.976	0.49	2002-12-21-23-23-55.250000	0.295	3372.2	47.722	7.522	7.95	0.5
2004-6-11-1-1-16.812500	8.4778	276.3	−20.872	10.288	0.972	1.346	2004-6-11-0-24-45.812500	0.1554	7041.3	51.756	10.082	0.062	0.886
2004-7-17-14-42-52.125000	9.7574	339	−12.366	10.754	−2.936	2.612	2004-7-17-14-15-8.000000	0.152	3277.4	31.366	10.306	−3.462	2.684

Table 1 (continued)

Time1	*N*1	*T*1	Bz1	*x*	*y*	*z*	Time0	*N*0	*T*0	Bz0	*x*	*y*	*z*
2005-1-25-17-58-45.250000	9.1104	245	−16.596	9.864	6.814	−1.196	2005-1-25-18-10-44.000000	0.236	5177.5	33.908	9.626	6.98	−1.032
2005-1-25-18-18-7.000000	14.0236	225.6	−16.024	9.478	7.084	−0.934	2005-1-25-18-14-7.250000	0.2152	5129.9	37.702	9.558	7.026	−0.986
2005-6-26-8-57-37.250000	7.5592	375.5	−19.414	10.082	0.062	2.08	2005-6-26-8-50-2.500000	0.1598	4818	37.446	10.03	−0.148	2.07
2005-6-26-8-59-13.000000	7.5714	367.4	−18.686	10.094	0.108	2.08	2005-6-26-9-3-12.750000	0.2376	2991	35.864	10.12	0.22	2.09
2005-6-26-9-12-47.000000	7.163	414	−17.21	10.178	0.488	2.1	2005-6-26-9-8-48.000000	0.2432	3559.2	34.914	10.152	0.378	2.1
2005-6-26-9-24-9.500000	3.2404	602.4	−20.244	10.244	0.808	2.11	2005-6-26-9-27-57.000000	0.084	6472.3	35.116	10.27	0.912	2.11
2009-3-16-4-30-11.500000	6.8206	322.3	−19.028	10.996	3.314	4.25	2009-3-16-4-24-12.500000	0.1284	4399.8	31.258	11.11	3.206	4.21
2009-3-16-4-31-47.125000	8.6992	235.5	−13.358	10.966	3.34	4.26	2009-3-16-4-37-10.375000	0.1432	4225.4	30.708	10.864	3.434	4.292
2009-4-26-20-50-43.250000	12.0854	252.1	−11.194	11.108	−3.564	1.088	2009-4-26-20-58-30.000000	0.2422	2739.6	42.08	11.07	−3.392	1.182
2009-4-26-21-2-5.250000	12.9446	249.8	−13.272	11.05	−3.316	1.226	2009-4-26-20-58-30.000000	0.2422	2739.6	42.08	11.07	−3.392	1.182
2009-4-26-21-57-31.750000	10.7382	284.5	−20.186	10.698	−2.124	1.928	2009-4-26-21-53-32.500000	0.1392	2769.6	42.648	10.726	−2.212	1.876
2009-4-26-22-17-40.000000	12.645	244.4	−16.016	10.54	−1.692	2.188	2009-4-26-22-12-41.000000	0.1684	3729.6	43.48	10.58	−1.802	2.124
2009-4-26-22-48-22.750000	11.3072	252.7	−17.796	10.256	−1.006	2.588	2009-4-26-22-50-58.000000	0.2948	1828.1	42.918	10.23	−0.948	2.622
2009-4-26-22-55-57.250000	15.5164	230.1	−22.048	10.18	−0.832	2.682	2009-4-26-22-51-34.000000	0.3632	1479.1	43.874	10.224	−0.932	2.628
2009-4-26-23-17-41.250000	12.3728	214.3	−18.692	9.956	−0.342	2.952	2009-4-26-23-22-4.750000	0.128	3653.3	41.588	9.906	−0.242	3.006
2009-5-7-8-22-31.562500	16.2594	267.8	−12.922	10.25	−2.102	2.49	2009-5-7-8-19-20.125000	0.2402	4938.3	47.132	10.26	−2.188	2.478
2009-5-7-8-32-5.875000	11.932	352.6	−17.23	10.2	−1.842	2.54	2009-5-7-8-27-42.625000	0.2568	3655.7	47.632	10.22	−1.962	2.52
2009-5-7-8-32-17.812500	12.1476	350.1	−17.252	10.2	−1.836	2.54	2009-5-7-8-35-41.250000	0.2892	2522.9	49.332	10.18	−1.742	2.55
2009-5-7-8-48-26.937500	13.1072	296.8	−14.3	10.11	−1.382	2.602	2009-5-7-8-53-2.125000	0.2434	3785.2	46.916	10.08	−1.256	2.62
2009-5-7-9-14-10.375000	15.8386	217.4	−28.102	9.95	−0.662	2.69	2009-5-7-9-9-59.125000	0.2168	4864.8	46.992	9.98	−0.78	2.68
2009-5-7-9-14-10.375000	15.8386	217.4	−28.102	9.95	−0.662	2.69	2009-5-7-9-17-57.687500	0.2532	5374.9	40.472	9.924	−0.558	2.702
2011-6-22-11-9-15.375000	5.5678	283.4	−21.244	9.95	0.322	1.632	2011-6-22-11-13-26.375000	0.0922	5416.9	42.408	9.938	0.418	1.564
2011-6-22-11-29-11.375000	7.1604	273.3	−26.372	9.87	0.792	1.314	2011-6-22-11-22-1.000000	0.1808	3867.4	42.338	9.9	0.618	1.426
2012-9-7-13-29-36.187500	11.7386	126	−31.36	9.23	1.392	−5.344	2012-9-7-13-25-49.000000	0.2008	6062.3	28.112	9.24	1.298	−5.284
2012-9-7-13-35-34.937500	10.2604	197	−25.042	9.21	1.538	−5.434	2012-9-7-13-40-10.000000	0.2798	5780.2	28.982	9.2	1.652	−5.504
2012-9-7-15-46-55.250000	6.2392	206.8	−21.574	8.474	4.91	−6.966	2012-9-7-15-38-9.125000	0.2324	6735.3	20.864	8.542	4.68	−6.896
2012-9-7-15-46-55.250000	6.2392	206.8	−21.574	8.474	4.91	−6.966	2012-9-7-15-51-18.312500	0.2886	5662.8	19.722	8.44	5.026	−7
2012-9-7-16-47-54.375000	5.1556	142.4	−29.852	7.97	6.532	−7.31	2012-9-7-16-26-34.875000	0.2194	6400.4	24.32	8.158	5.968	−7.22
2014-4-28-22-49-13.750000	13.1522	145.1	−18.46	10.266	6.46	1.88	2014-4-28-22-59-47.250000	0.2464	4559.3	30.184	10.034	6.588	1.89
2015-8-16-5-56-28.125000	8.1206	292.3	−36.392	8.102	2.904	−2.98	2015-8-16-5-33-10.000000	0.4772	5524.6	47.854	8.304	2.266	−2.94
2015-8-16-6-20-34.125000	6.7596	348.4	−34.956	7.864	3.544	−3.03	2015-8-16-6-47-15.500000	0.4228	4546.4	44.322	7.554	4.242	−3.082
2015-8-26-18-39-37.000000	5.759	289.8	−51.698	7.584	5.548	−1.812	2015-8-26-18-29-51.250000	0.368	6146.9	54.636	7.702	5.276	−1.89
2015-8-26-18-39-37.000000	5.759	289.8	−51.698	7.584	5.548	−1.812	2015-8-26-18-47-47.000000	0.462	4924.4	55.73	7.486	5.778	−1.748
2015-8-26-19-7-42.250000	6.507	181.3	−54.996	7.23	6.318	−1.57	2015-8-26-18-47-47.000000	0.462	4924.4	55.73	7.486	5.778	−1.748

Table 1 (continued)

Time1	*N*1	*T*1	Bz1	*x*	*y*	*z*	Time0	*N*0	*T*0	Bz0	*x*	*y*	*z*
2015-8-26-19-25-14.000000	9.2328	172.3	−52.866	6.996	6.778	−1.402	2015-8-26-19-43-57.250000	0.5622	4913.5	45.382	6.73	7.244	−1.22
2015-8-26-20-1-5.000000	6.0098	187.2	−46.086	6.474	7.664	−1.048	2015-8-26-19-53-55.000000	0.5674	4975.8	40.406	6.582	7.488	−1.12
2015-8-26-20-15-14.000000	8.7524	175.6	−45.442	6.256	7.99	−0.898	2015-8-26-20-6-28.000000	1.1994	5269.5	45.114	6.394	7.788	−0.988
2016-9-14-21-29-15.250000	7.1692	299.6	−38.07	8.882	−4.638	−1.662	2016-9-14-21-58-20.000000	0.1678	4882.3	53.612	9.118	−3.856	−1.51
2016-9-14-22-54-5.750000	10.6072	164.2	−56.78	9.458	−2.316	−1.15	2016-9-14-22-8-29.250000	0.3312	2873.6	52.716	9.19	−3.582	−1.45
2016-9-14-22-54-5.750000	10.6072	164.2	−56.78	9.458	−2.316	−1.15	2016-9-14-23-13-0.000000	0.2358	5302	63.44	9.53	−1.786	−1.02
2016-9-14-23-38-29.625000	9.1386	365.8	−64.864	9.61	−1.072	−0.83	2016-9-14-23-21-45.875000	0.2802	5935.8	60.846	9.566	−1.542	−0.956
2016-9-14-23-38-29.625000	9.1386	365.8	−64.864	9.61	−1.072	−0.83	2016-9-14-23-49-27.000000	0.2684	6496.7	60.852	9.63	−0.766	−0.754
2016-9-15-0-21-7.000000	6.718	326.6	−61.22	9.64	0.132	−0.53	2016-9-15-0-14-56.500000	0.3048	5859.1	65.572	9.64	−0.042	−0.576
2016-9-15-0-21-7.000000	6.718	326.6	−61.22	9.64	0.132	−0.53	2016-9-15-0-28-29.000000	0.4196	5645.1	58.772	9.64	0.346	−0.48
2018-7-29-2-19-50.000000	8.0668	209.9	−27.354	11.042	2.416	−1.59	2018-7-29-2-47-18.000000	0.1862	5395	45.486	10.656	2.976	−1.426
2019-7-2-14-22-19.953125	11.015	175.6	−31.718	7.572	7.736	−0.176	2019-7-2-14-34-4.593750	0.5458	3892	31.478	7.288	7.86	−0.06

Acknowledgements
S.N. would like to especially thank Ippon-Kakou-Kai for motivation.

Author contributions
KK and SN conceived the idea of the study. KK significantly contributed to data analysis and interpretation. All authors critically reviewed and revised the manuscript draft and approved the final version for submission.

Funding
This study is supported by MEXT/JSPS KAKENHI under Grant No. 21K03645.

Availability of data and availability
Publicly available datasets were analyzed in this study. This data can be found here: http://cdaweb.gsfc.nasa.gov/istp_public/.

Declarations

Competing interests
The authors declare that they have no conflict of interest.

Author details
[1]Research Center for Space and Cosmic Evolution, Ehime University, Matsuyama, Ehime 790-8577, Japan. [2]Tsukuba University of Technology, 4-3-15 Amakubo, Tsukuba 305-8520, Japan. [3]Solar Science Observatory, National Astronomical Observatory of Japan, 2-21-1 Osawa, Mitaka, Tokyo 181-8588, Japan. [4]Institute of Space and Astronautical Science, Japan Aerospace Exploration Agency, 3-1-1 Yoshinodai, Chuo-ku, Sagamihara, Kanagawa 252-5210, Japan.

Received: 26 July 2023 Accepted: 22 January 2024
Published online: 20 February 2024

References

Archer MO, Hietala H, Hartinger MD, Plaschke F, Angelopoulos V (2019) Direct observations of a surface eigenmode of the dayside magnetopause. Nat commun. https://doi.org/10.1038/s41467-018-08134-5
Cassak PA, Shay M (2007) Scaling of asymmetric magnetic reconnection: general theory and collisional simulations. Phys Plasmas 14:10
Chen H, Zhang J, Cheng X, Ma S, Yang S, Li T (2014) Direct observations of Thether-cutting reconnection during a major solar event from 2014 February 24 to 25. ApJL 797:L15
Gosling JT, Thomsen MF, Bame SJ, Russell CT (1986) Accelerated plasma flows at the near-tail magnetopause. J Geophys Res 91:3029–3041
Hasegawa H, Fujimoto M, Maezawa K, Saito Y, Mukai T (2003) Geotail observations of the dayside outer boundary region: interplanetary magnetic field control and dawn-dusk asymmetry
Hoshino M, Nishida A (1983) Numerical simulation of the dayside reconnection. J Geophys Res 88(A9):6926–6936
Ivchenko NV, Sibeck DG, Takahashi K, Kokubun S (2000) A statistical study of the magnetosphere boundary crossings by the Geotail satellite. Geophys Res Lett 27(18):2881–2884
Kokubun S, Yamamoto T, Acuna MH, Hayashi K, Shiokawa K, Kawano H (1994) The GEOTAIL magnetic field experiment. J Geomagn Geoelectr 46:7–21
Kondoh K, Ugai M, Shimizu T (2004) The dynamics of plasmoid in asymmetric spontaneous fast reconnection. Adv Space Res 33(5):794–798
Lin Y, Lee LC (1993) Structure of reconnection layers in the magnetosphere. Space Sci Rev 65:59
Mukai T, Machida S, Saito Y, Hirahara M, Terasawa T, Kaya N, Obara T, Ejiri M, Nishida A (1994) The low energy particle (LEP) experiment onboard the GEOTAIL satellite. J Geomagn Geoelectr 46:669–692
Nitta S, Wada T, Fuchida T, Kondoh K (2016) Critical differences of asymmetric magnetic reconnection from standard models. ApJ 828:63
Nitta S, Kondoh K (2019) Properties of extremely asymmetric magnetic reconnection. ApJ 872:142
Nitta S, Kondoh K (2021) Fundamental properties of sheared/guide field MHD magnetic reconnection. ApJ 907:21
Nitta S, Kondoh K (2022) Effects of magnetic shear and thermodynamic asymmetry on spontaneous magnetohydrodynamic reconnection. ApJ 936:125
Parker E (1963) The solar-flare phenomenon and the theory of reconnection and annihiliation of magnetic fields. ApJS 8:177
Paschmann G, Sonnerup BUÖ, Papamastorakis I, Sckopke N, Haerendel G, Bame SJ, Asbridge JR, Gosling JT, Russell CT, Elphic RC (1979) Plasma acceleration at the Earth's magnetopause: evidence for reconnection. Nature 282:243–246
Petschek HE (1964) Magnetic field annihilation. In: Hess WN (ed) The physics of solar flares. NASA, Washington, DC, p 425
Petschek HE, Throne RM (1967) The existence of intermediate waves in neutral sheets. ApJ 147:1157
Phan TD, Freeman MP, Kistler LM, Klecker B, Haerendel G, Paschmann G, Sonnerup BUÖ, Baumjohann W, Bavassano-Cattaneo MB, Carlson CW, DiLellis AM, Fornacon K-H, Frank LA, Fujimoto M, Georgescu E, Kokubun S, Moebius E, Mukai T, Paterson WR, Reme H (2001) Evidence for an extended reconnection line at the dayside magnetopause. Earth Planets Space 53:619–62
Phan TD, Gosling JT, Oieroset M, Fujimoto M, Drake JF, Angelopoulos V (2013) The dependence of magnetic reconnection on plasma β and magnetic shear: Evidence from magnetopause observations. Geophys Res Lett 40:11–16
Teh W-L, Hau L-N (2004) Evidence for pearl-like mangetic island structures at dawn and dusk side magnetopause. Earth Planets Space 56:681–686
Tsuneta S (1996) Structure and dynamics of magnetic reconnection in a solar flare. ApJ 456:840
Walsh BM, Sibeck DG, Wang Y, Fairfield DH (2012) Dawn-dusk asymmetries in the Earth's magneto sheath. J Geophys Res 117:A12211. https://doi.org/10.1029/2012JA018240

Publisher's Note